Article

# Two-Dimensional Ultrathin CeVO$_4$ Nanozyme: Fabricated through Non-Oxidic Material

Kuldeep Kumar, Tanmoy Maity, Leela S. Panchakarla, and Siddarth Jain*

Read Online

ACCESS | Metrics & More | Article Recommendations | Supporting Information

**ABSTRACT:** In recent years, the synthesis of materials in lower dimensions, like two-dimensional (2D) or ultrathin crystals, with distinctive characteristics has attracted substantial scientific attention. The mixed transition metal oxides (MTMOs) nanomaterials are the promising group of materials, which have been extensively utilized for various potential applications. Most of the MTMOs were explored as three-dimensional (3D) nanospheres, nanoparticles, one-dimensional (1D) nanorods, and nanotubes. However, these materials are not well explored in 2D morphology because of the difficulties in removing tightly woven thin oxide layers or exfoliations of 2D oxide layers, which hinder the exfoliation of beneficial features of MTMO. Here, through the exfoliation via Li$^+$ ion intercalation and subsequent oxidation of CeVS$_3$ under hydrothermal condition, we have demonstrated a novel synthetic route for the fabrication of 2D ultrathin CeVO$_4$ NS. The as-synthesized CeVO$_4$ NS exhibit adequate stability and activity in a harsh reaction environment, which gives excellent peroxidase-mimicking activity with a $K_M$ value of 0.04 mM, noticeably better than natural peroxidase and previously reported CeVO$_4$ nanoparticles. We have also used this enzyme mimic activity for the efficient detection of biomolecules like glutathione with a LOD of 53 nM.
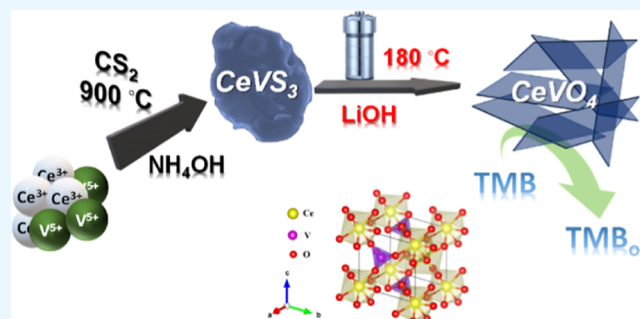
## INTRODUCTION

In recent years, significant strides have been made in the synthesis of a variety of 2D nanomaterials such as graphene,[1−4] metal chalcogenides,[5,6] metal oxides,[7,8] metal hydroxides,[9,10] and halide perovskites.[11,12] Such materials possess unique chemical and physical properties which are not present in their bulk analogues, as well as in higher dimensional nanostructures.[13−15] Notably, mixed transition metal oxides (MTMOs) nanomaterial exhibits higher catalytic activity than their single-element counterparts (monometallic oxides), owing to the additive and synergistic effects of the different metal components.[16] The presence of multi-metallic active sites enhances the catalytic characteristics and selectivity of such materials for a wide range of chemical transformations. In addition, the small activation energy for the electron transfer between the cations enable these MTMOs to exhibit better electrical conductivity than simple TMOs. Therefore, MTMO nanostructures have been extensively explored as potential possibilities for photo-catalysis,[17−19] electro-catalysis,[20,21] and power storage,[22] due to their mixed oxidation state and abundant redox reactions.[23] As of now, MTMOs are most commonly investigated in the form of 0D nanoparticle[24,25] or 1D nanowires or nanotubes[26,27] and 3D nanoclusters or microspheres.[28] On the contrary, the 2D or ultrathin crystal (particularly a few layers thick) nanostructured MTMOs are less investigated.[29,30] The fabrication of 2D nanostructures from MTMO materials offers great potential for improving various energy-related aspects, including alkali ion storage, electrode materials for alkali-ion batteries, effective oxygen reduction reaction electrocatalysts for metal−air batteries and fuel cells, as well as electrochemical capacitors, and so forth.[17] Similar to other conventional 2D materials, MTMOs are expected to exhibit unique properties that will allow the construction of multifunctional electronic devices. However, the difficulty of controlling the exfoliation of three-dimensional oxide crystals or removing strongly bonded thin oxide layers from the substrate prevents this possibility.[31]

Among the lanthanide-based orthovanadate, cerium vanadate (CeVO$_4$) is a well-known semiconducting material that has been widely explored due to its magnetic, catalytic, optical, large specific surface area, and exceptional electrochemical behavior.[32−35] Owing to its 4f electronic structure and various electronic transition modes, CeVO$_4$ has shown redox as well as optical properties. CeVO$_4$ nanoparticles have been employed in a variety of applications, including gas sensors,[36,37] photocatalysts,[38,39] luminescence,[40] lubricant additives,[41] elec-
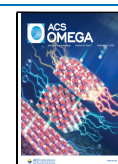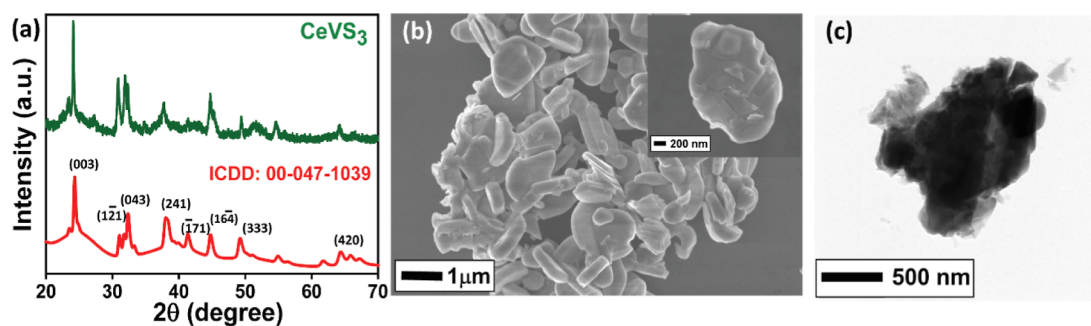
**Figure 1.** (a) PXRD spectra of bulk $CeVS_3$; (b) SEM image; inset showing high resolution SEM image, and (c) TEM image of as obtained $CeVS_3$ under $CS_2/H_2$ atmosphere at 900 °C.
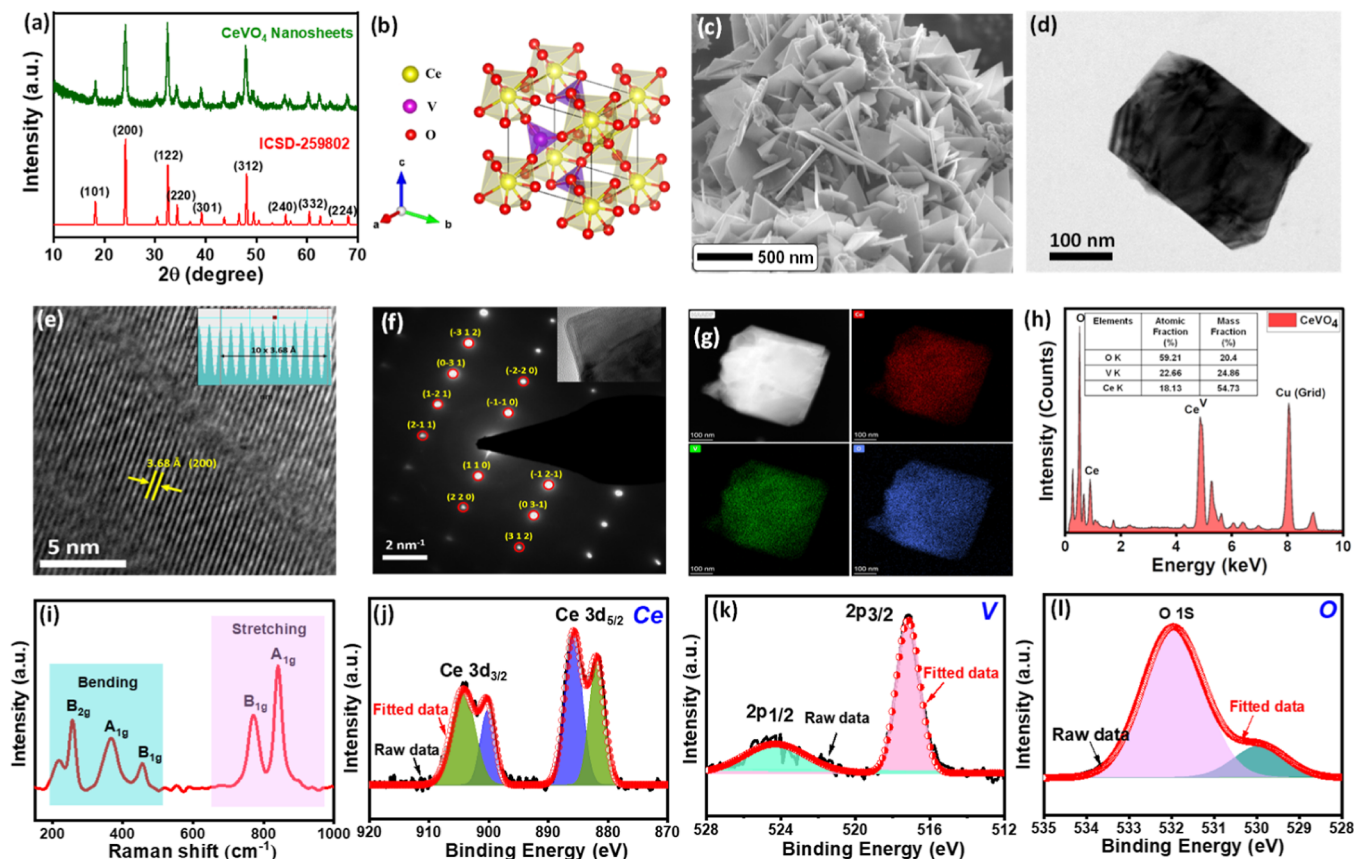


**Figure 2.** (a) PXRD spectra of ultrathin $CeVO_4$ NS, (b) $CeVO_4$ crystal structure, (c) SEM image, (d) TEM image, (e) HRTEM image, (f) SAED pattern of corresponding TEM image, (g) elemental mapping, (h) EDX spectrum, (i) Raman spectrum, and high-resolution XPS spectrum of as-prepared ultrathin $CeVO_4$ NS: (j) Ce 3d, (k) V 2p, and (i) O 1s (binding energy is calculated with respect to C 1s, 284.6 eV).

trochromic materials,[42] and batteries.[43] Consequently, there has been a lot of focus on developing methods for efficiently generating $CeVO_4$ nanomaterials with a desired morphology.[44] All previously reported methods require layered oxide materials for the synthesis of 2D morphology; however, there is another way to produce oxide products from non-oxidic materials. Interestingly, recent studies suggest that the fabrication of non-oxide NS and subsequent oxidation are plausible. For example, recently, Rh NS was converted to $Rh_2O_3$ NS by chemical oxidation using $HClO$.[45] Other efforts have demonstrated the oxidation of large surfaces to leverage the features of two-dimensional sheets, as demonstrated for $CuO/Cu_2O$ on a Cu surface (electrochemically via anodization).[46]

In recent years, metal oxide-based micro-/nano-structures have gained immense attention because of their simple synthesis and natural enzyme-like activity. Typically, natural enzyme-catalyzed reactions are very sensitive to reaction conditions and varying from the optimal condition often tends to reduce their activity.[47] Also, degradation under harsh reaction conditions and difficulties in recycling, preparation, and purification severely restrict the practical application of natural enzymes.[48,49] Whereas, metal oxide-based nanostructured materials with potential enzyme mimetic activity are often recyclable, offer high activity, and also retain their activity in harsh reaction conditions.[50,51] On the contrary, morphologically controlled metal oxide-based nanomaterials offer a viable alternative for natural enzymes in a wide range of applications.[52,53] Due to the important catalytic activity and

potential applications of peroxidase, several metal oxide nanomaterials mimicking peroxidase-like activity have been reported. Various transition metal oxides, such as $CeO_2$ nanostructures,[54] $CeVO_4$ nanorods,[55] and $Cu_3V_2O_7(OH)_2$[56] were reported to exhibit peroxidase-like catalytic activity. Although these materials exhibit efficient peroxidase mimetic activity, the surfactants involved during synthesis, multi-step procedure, and limited number of active sites severely impede us to take their full benefits for different applications.

Previously, liquid exfoliation emphasized on layered materials such as metal sulfides ($MoS_2$), GO, and metallates, which can be easily exfoliated into two-dimensional thin layers due to weak van der Waals forces between stacking layers and linkage of all in-plan atoms via strong chemical bonding.[8,57] However, exfoliation of non-layered material especially metal oxide with the general formula $ABO_3$ (perovskite type) and $ABO_4$ (monoclinic or tetragonal type) is an extremely challenging task due to strong chemical bonding between all the atoms, resulting in dangling bonds along the edges or on the surface, thereby tempting high energy surfaces, which facilitate uniform growth in all directions. Therefore, it is imperative and highly beneficial to create an effective and simple method for the large-scale production of 2D oxides. Here, we have synthesized ultrathin $CeVO_4$ nanosheets (NS) through facile two-step synthesis, via non-oxidic materials. We initially synthesized $CeVS_3$ bulk sheets by a solid-state synthesis at 900 °C under $CS_2/H_2$ condition, which was further oxidized and exfoliated hydrothermally in the presence of LiOH at an elevated temperature. Due to the presence of multivalent catalytic sites of Ce and V, the ultrathin 2D bimetallic oxide NS displayed improved redox activities, which resulted in enormously effective peroxidase activity. The enzyme mimicking activity of the $CeVO_4$ NS was implied to develop a sensitive colorimetric glutathione detection system. The findings show that the $CeVO_4$ NS could have potential and diverse applications in biotechnology, catalysis, and clinical diagnostics. Also, the oxidation and subsequent exfoliation of $CeVS_3$ bulk sheets into ultrathin $CeVO_4$ NS are expected to introduce a new dimension with excellent control of the interfacial features for multifunctional applications.

## ■ RESULTS AND DISCUSSION

In this work, we employed a straightforward two-step method for the synthesis of ultrathin-2D $CeVO_4$ nanosheets (NS) from non-oxidic material (sulfide). First, we fabricated $CeVS_3$ bulk sheets by a solid-state synthesis at 900 °C under $CS_2/H_2$ atmosphere and then oxidized and exfoliated these $CeVS_3$ bulk sheets hydrothermally in the presence of LiOH. The obtained materials were characterized by means of various spectroscopic and microscopic techniques. The powder X-ray diffraction (PXRD) pattern of as-synthesized $CeVS_3$ (Figure 1a) illustrated the pure $CeVS_3$ phase of material (ICDD 047-1039). The intense Bragg's peaks in XRD patterns infer the crystalline nature of the material. The scanning electron microscopy (SEM) image of $CeVS_3$ (Figure 1b) depicted bulk sheets or stacked sheet-like morphology of $CeVS_3$ with an average size of 1 $\mu$m, which was further confirmed by transmission electron microscopy (TEM) analysis (Figure 1c). Energy dispersive X-ray (EDX) and elemental mapping were utilized to study chemical composition and elemental distribution of the $CeVS_3$ matrix (Figure S1), revealing a homogeneous distribution of Ce, V, and S.

The pure-phased $CeVS_3$ was then subjected to exfoliation oxidation for $CeVO_4$ synthesis under hydrothermal condition. The phase purity and structural composition of $CeVO_4$ NS were analyzed using PXRD analysis (Figure 2a). The PXRD pattern of the obtained material displayed various diffraction patterns which are perfectly aligned to the tetragonal (Figure 2b) $CeVO_4$ crystal structure (zircon type, ICSD no. 259802). The PXRD spectra showed no other anomalous peaks, indicating the complete oxidation of $CeVS_3$ to $CeVO_4$. The SEM study (Figure 2c) revealed the formation of nanosheet-like structure having an average size and thickness of 500 and 20 nm, respectively. It can be seen that the homogeneous distribution of sheet-like structures was observed without any additional nanostructures in the matrix of the $CeVO_4$. The TEM images of the as-prepared material (Figure 2d) depicts sheet-like structures with an average length of ∼300 nm and a thickness of ∼15 nm, which is in good agreement with the results of SEM.

High resolution transmission electronic microscopy (HRTEM) images of the $CeVO_4$ NS (Figure 2e) demonstrate distinct lattice fringes parallel to one another with the same lattice spacing ($d$ value) of 3.68 Å, resembling the inter-planar spacing of the (200) lattice plane of the tetragonal (zircon type) $CeVO_4$ crystal structure. The selected area electron diffraction (SAED) pattern displays (Figure 2f) discrete spots that correspond to the tetragonal $CeVO_4$ structure. TEM−EDX spectrum analysis validated the presence of Ce, V, and O elements in the obtained material, whereas elemental mapping analysis confirmed the uniform distribution of Ce, V, and O elements (Figure 2g−h). Raman spectroscopy was employed to analyze the $CeVO_4$ NS's structural details (Figure 2i). The symmetric ($A_{1g}$) and anti-symmetric ($B_{1g}$) stretching of $VO_4^{3-}$ tetrahedrons are represented by peaks at 840.9 and 771 cm$^{-1}$, respectively, whereas $B_{1g}$ and $A_{1g}$ bending modes are represented by peaks at 455.5 and 366 cm$^{-1}$, respectively. The external mode of Ce-$VO_4$ vibration occurs below the peak at 259 cm$^{-1}$, which is associated with the $B_{2g}$ bending mode of $VO_4^{3-}$ tetrahedrons.[58] To understand more about the oxidation state of the elements in as-prepared ultrathin $CeVO_4$ crystals, X-ray photoelectron spectroscopy (XPS) analysis was performed. Peaks corresponding to the elements Ce 3d, V 2p, and O 1s in the full range survey spectrum (Figure S2) reveal the chemical purity of the as-prepared ultrathin $CeVO_4$. The high-resolution XPS spectra (Figure 2j) revealed two distinctive peaks at 904.2 and 900.3 eV, which are associated with the Ce 3d$_{3/2}$. Furthermore, two peaks correspond to Ce 3d$_{5/2}$ peaks appearing at around 885.9 and 881.8 eV. In other words, the appearance of these four peaks demonstrates that Ce$^{3+}$ center is indeed present.[59] Also, the core spectrum of V 2p deconvolutes into two peaks at 524.4 and 517.1 eV, which designates the V 2p$_{1/2}$ and V 2p$_{3/2}$ states, respectively (Figure 2k).[60] High-resolution O 1s signal deconvolution suggests the presence of two peaks at 531.7 and 529.6 eV (Figure 2l). The peak at 530.7 eV corresponds to the existence of surface lattice oxygen; in contrast, the presence of OH groups on the surface of $CeVO_4$ is indicated by the peak at 528.6 eV.[55]

The formation of ultrathin $CeVO_4$ NS was carried out through a solid-state synthesis of $CeVS_3$ followed by the liquid exfoliation of as-prepared $CeVS_3$ and subsequent in situ oxidation under the hydrothermal condition at 180 °C in the presence of LiOH. The previously published procedures necessitate the use of layered oxide materials; however, there
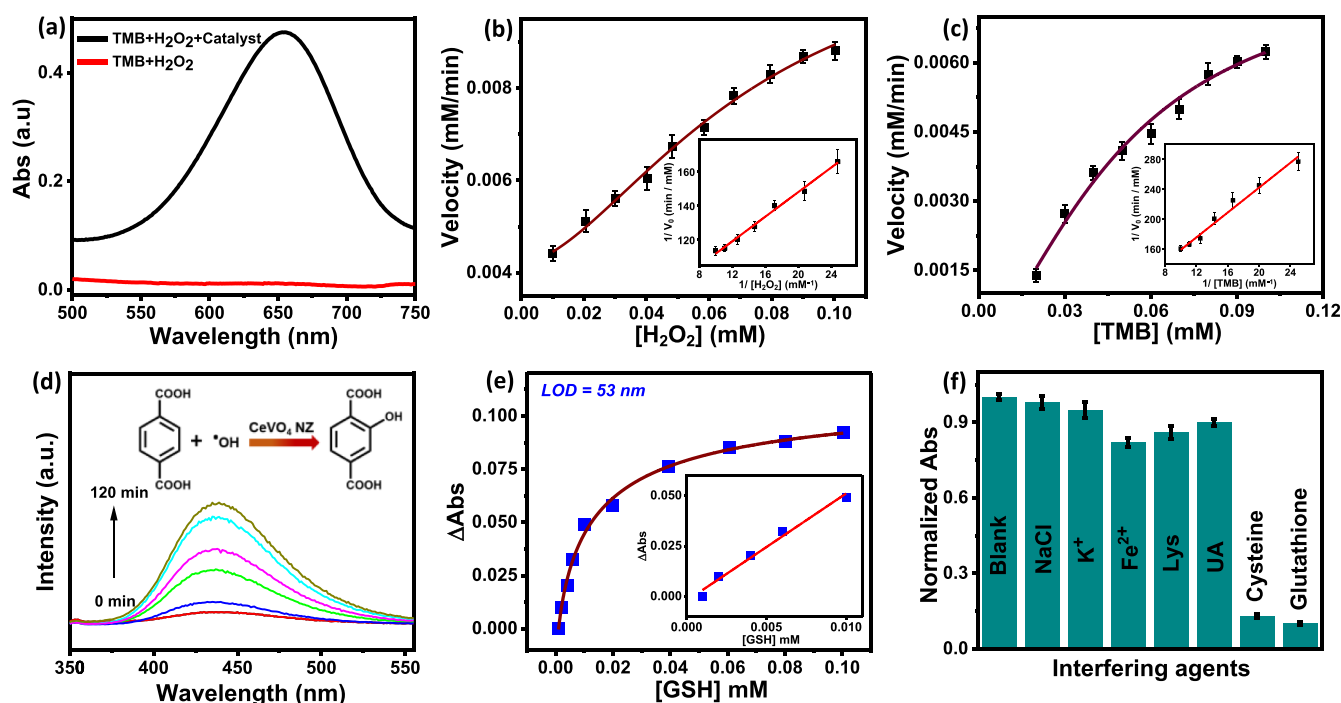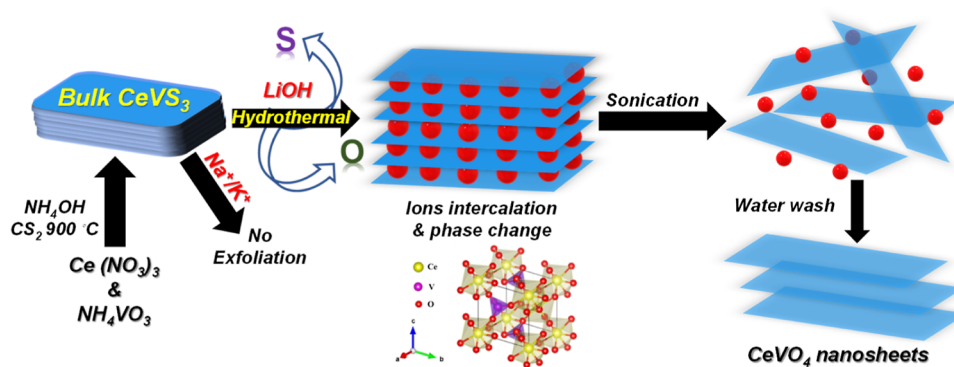
**Scheme 1. Schematic Representation of Fabrication of CeVO$_4$ NS.**





**Figure 3.** (a) UV−visible spectra ultrathin CeVO$_4$ NS catalyzed TMB oxidation in the presence or absence of H$_2$O$_2$; (b) UV−visible steady-state kinetic investigation of ultrathin CeVO$_4$ NS at a fixed TMB concentration (0.1 mM) and varying H$_2$O$_2$ concentration; (c) UV−visible steady-state kinetic investigation of ultrathin CeVO$_4$ NS at a constant concentration of H$_2$O$_2$ (1 mM), as well as different concentrations of TMB; (insets of b,c) double-reciprocal graphs of CeVO$_4$ activity at changing concentrations of the other substrate vs a constant concentration of the first substrate (TMB and H$_2$O$_2$); (d) schematic showing hydroxyl radical-catalyzed terephthalic acid oxidation and time-dependent fluorescence spectrum; (e) effect of glutathione concentration on the CeVO$_4$ nanozyme activity. The inset figure shows the linear dependence of absorbance change with a lower range of glutathione concentration. (f) Effect of different interfering agents on the peroxidase mimicking activity of CeVO$_4$ nanozyme.

is another approach for producing oxide products from non-oxidic materials. The transformation of metal sulfides into metal oxides is carried out by oxidation leaching in alkaline solution relied on the change of thermodynamic parameters such as Gibbs free energy and the equilibrium constant.[61] It also has mentioned that intercalation and exfoliation are two processes that may involve structural shifts, phase transitions, and chemical reactions.[62,63] Therefore, we assume that, during the process, Li$^+$ ions are intercalated inside CeVS$_3$ layers. As a result, the bonding link between the CeVS$_3$ layers was weakened, which caused the layers to exfoliate. It is feasible for sulfur to leach out from CeVS$_3$ and transform it into a thermodynamically stable tetragonal zircon type phase of CeVO$_4$ in an aqueous medium under hydrothermal conditions (Scheme 1).[64] In addition, sheet-like structures were unable to be produced when Li$^+$ was absent from the reaction media.

These findings lend credence to the hypothesis that Li$^+$ is indispensable to the formation of sheet-like structures. To validate the role of lithium ions, similar reactions were performed using NaOH and KOH, while retaining other parameters constant. Based on the obtained results, it may be argued that the formation of ultrathin CeVO$_4$ NS did not take place in the presence of K$^+$ and Na$^+$ (Figure S3). The disparity in the radii of these ions as compared to one another might be a potential cause of that phenomenon. The ionic radii of Na$^+$ and K$^+$ are both bigger (0.102 and 0.138 nm, respectively) than those of Li$^+$ (0.076 nm).[65]

**Peroxidase Mimicking Activity of CeVO$_4$ NS.** In recent years, metal oxide-based nanomaterials with enzyme-mimetic capabilities have gained immense attention because of their simple synthesis and capacity to withstand strong reaction conditions. Nanomaterials based on 2D metal oxides have the

potential to be utilized in a wide variety of applications as a viable substitute for natural enzymes.[50−52,56,66−69] The peroxidase mimicking activity of ultrathin CeVO$_4$ NS is investigated by using 3,3,5,5′-tetramethylbenzidine (TMB) as a substrate where the oxidized product of TMB showed an intense absorbance peak at 652 nm (Figures S4,S5). We have investigated the peroxidase mimicking activity of the as-synthesized CeVO$_4$ NS by performing the CeVO$_4$ NS catalyzed oxidation of TMB in the presence of hydrogen peroxide (H$_2$O$_2$), and the reaction progress was monitored using UV−visible spectroscopy. It was observed that the H$_2$O$_2$ + TMB systems showed no absorption peak. However, the H$_2$O$_2$ + TMB + CeVO$_4$ NS system showed a strong absorption peak at around 652 nm (Figure 3a), signifying the effective peroxidase-like behavior of CeVO$_4$ NS. To achieve an optimum activity, influence of pH on CeVO$_4$ NS catalytic activities was studied at room temperature in sodium acetate buffer (100 mM) over a pH range of 2 to 10. The response curves (Figure S6) indicate that pH 4.0 was found to be an ideal condition where maximum activity was observed, which resembles (HRP) operating conditions. The impact of catalyst concentration on nanozyme activity was also studied using a concentration-dependent study. It was found that the catalytic activity linearly increased with the concentration of CeVO$_4$ NS (Figure S7). To comprehend the kinetic performance of the system, the reaction rate of CeVO$_4$ NS was determined using variable concentrations of TMB and H$_2$O$_2$ in this system, respectively. From Figure 3b,c, it can be easily seen that, at the lower substrate concentration range, the rate of the CeVO$_4$ NS catalyzed reaction increased linearly. Nonetheless, a lesser shift in the reaction rate is seen at higher substrate concentration. This suggests that the CeVO$_4$ NS catalyzed reaction follows typical Michaelis−Menten model curves for H$_2$O$_2$ and TMB as substrates in a given range of concentrations.

The Michaelis−Menten kinetics of CeVO$_4$ nanozyme catalyzed reactions are also further supported by the linear Lineweaver−Burk plot (inset Figure 3b,c). Using the Michaelis−Menten equation or Lineweaver−Burk plot, the Michaelis constant ($K_M$), an indication of enzyme affinity for its substrate, was determined. We found $K_M$ values of 0.04 and 0.05 mM for H$_2$O$_2$ and TMB as substrates, respectively, which is considerably lower compared to the natural peroxidase enzyme, and earlier reported CeVO$_4$ nanomaterials.[70] The lower $K_M$ value associated with CeVO$_4$ NS suggests the stronger affinity of the substrate to the CeVO$_4$ compared to natural horseradish peroxidase (HRP). Additionally, we found that the CeVO$_4$ NS developed in this study had a substantially lower $K_M$ value than earlier published nanozymes exhibiting intrinsic peroxidase activity. The $V_{max}$ value of our nanozyme was better than other reported works and three times higher than HRP, indicating the superior peroxidase activity of CeVO$_4$ NS (Table S1). The high peroxidase activity of the CeVO$_4$ NS can be ascribed to the presence of the bimetallic nature of the catalyst along with more exposed sites on its surface.[71] The as-prepared material has a zeta potential of −29.5 mV (Figure S8), indicating a negatively charged surface of the catalyst with a higher interaction with positively charged TMB, facilitating the quick catalytic process. The positively charged TMB molecules easily adsorb on the negatively charged surface of CeVO$_4$ NS and act as chromogenic e$^−$ donors. The amino groups of TMB molecules would donate electrons a lone pair to the ultrathin CeVO$_4$ NS surface, increasing the mobility and density of electrons there. As a

result, faster electron transfer occurs from CeVO$_4$ NS to H$_2$O$_2$ thereby accelerating the production of $^•$OH radical in the reaction medium. Furthermore, fluorescent probes were utilized to monitor CeVO$_4$ NS catalyzed formation of $^•$OH radicals, which has been proven as the source of peroxidase mimic catalytic activity through H$_2$O$_2$ breakdown. As a probe, a faintly fluorescent terephthalic acid was used in the experiment, which yields a highly fluorescent adduct (i.e., hydroxyl terephthalic acid) when coupled with $^•$OH radicals. As the reaction progresses in the presence of CeVO$_4$ NS and H$_2$O$_2$, there is a significant increase in the fluorescence intensity of terephthalic acid (at 440 nm), indicating the production of free radicals (Figure 3d). These results demonstrate the efficiency of CeVO$_4$ NS to produce $^•$OH radicals during the catalytic process, which is primarily responsible for their peroxidase-mimicking activity.[56] Additionally, in order to probe catalytic reaction center, the detailed HR-XPS study of CeVO$_4$ NS has been carried out before and after the catalytic reaction (Figure S9). After the reaction, a prominent peak for Ce$^{+4}$ is observed at 916 eV in the HR-XPS spectrum of Ce, which validates the involvement of the cerium as an active center toward peroxidase mimicking activity.

To investigate the influence of temperature on the nanozyme activity, we also performed the reaction at different reaction temperatures ranging from 20 to 50 °C. The obtained results suggest that the activity of the CeVO$_4$ nanozyme is strongly influenced by the reaction temperature. HRP activity began to decrease with rising temperatures and was completely lost once the temperature reached 60 °C (Figure S10). At higher temperatures (>80 °C), however, CeVO$_4$ NS maintained its activity at a steady 70%. This finding suggests the robustness of the CeVO$_4$ NS at high temperatures. Reusability and stability are important properties for continuous application with reduced costs. The recyclability of the catalyst was also evaluated, and results suggest that the activity of the catalyst is retained even after the 10th cycle (Figure S11).

The peroxidase mimicking activity of CeVO$_4$ nanozyme is also used for the sensitive detection of glutathione. Glutathione (GSH) is an important biomolecule and plays a vital role in mammalian and eukaryotic cells by protecting cells from reactive oxygen species (ROS) and toxins. The imbalance between GSH to GSSH (oxidized glutathione) suggests that the cells suffer from oxidative stress, and deviation of the ratio of GSH to GSSG from its standard range is associated with various clinical diseases.[66,72−75] Therefore, GSH can be used as clinical biomarkers and sensitive detection of GSH would provide us with point-of-care (PoC) diagnostics for numerous diseases. Because of the presence of free thiol groups in reduced glutathione, it exhibits important reducing properties. Here, a blue-colored oxidized TMB was used as an indicator for glutathione sensing. The addition of glutathione facilitates the reduction of blue-colored ox-TMB to colorless TMB. To investigate the effect of glutathione, we have performed CeVO$_4$ catalyzed oxidation of TMB (0.1 mM) in the presence of H$_2$O$_2$ (1 mM) and different concentrations of glutathione ranging from 0 to 100 $\mu$M. The result suggests that with an increase in glutathione concentration, the absorbance value decreases. We have recorded the absorbance value of the reaction system at 652 nm, and the change in decreasing absorbance value from the control ($\Delta A$) was plotted against the concentration of glutathione. From Figure 3e, it is observed that at the lower concentration range, the $\Delta A$ value increases linearly with

increasing glutathione concentration. After that, the $\Delta A$ value tends to saturate, which suggests that the effect of glutathione is more prominent at lower concentration ranges and the system becomes less sensitive at higher concentrations of glutathione. The inset Figure 3e (inset) shows a linear relation between GSH concentration and $\Delta A$ in a concentration range of 0 to 10 $\mu M$, and from the linearly fitted graph, we have calculated the limit of detection (LOD) by using the $3\sigma/s$ formula (where $\sigma$ is the standard deviation and $s$ is the slope). The LOD is found to be 53 nM, which suggests the potential of the nanozyme for sensitive GSH detection. Nevertheless, the sensitive colorimetric detection of GSH using the nanozyme system provides an important route for biomedical research. Furthermore, we also investigated the $CeVO_4$ nanozyme activity in the presence of different interfering agents like cysteine, uric acid, NaCl, KCl, and so forth. The results (Figure 3f) suggest inhibited catalytic activity of $CeVO_4$ nanozyme in the presence of biomolecules containing free thiol groups (i.e., cysteine and glutathione). In all, our synthesized $CeVO_4$ nanozyme demonstrates robust catalytic activity and notable reusability for on-field practical application. Further, the structural and compositional stability of the catalyst was also evaluated even after the catalytic experiment using XPS, SEM, and XRD analyses (Figures S9,S12). Results revealed sheet-like morphology with phase retention, inferring no structural and compositional change even after the 10 consecutive catalytic cycles.

## CONCLUSIONS

In conclusion, we demonstrate a novel method for the synthesis of 2D ultrathin $CeVO_4$ NS from the exfoliation and subsequent oxidation of $CeVS_3$. Unlike typical 2D layered structure materials such as $MoS_2$, metalates, and graphene, we established a unique synthesis technique for the fabrication of 2D ultrathin sheets of non-layered $CeVO_4$ with a 3D tetragonal crystal system in this study. Another important feature of this synthesis is that it involves one step in-situ oxidation of metal sulfides to metal oxides under hydrothermal exfoliation process. The obtained product has excellent phase purity (tetragonal zircon-type) with flat and smooth surfaces, and its migration onto substrates for further analysis is simple and flexible. The as-prepared material was explored for peroxidase-like activity. Multiple valence sites, synergistic effects amongst metal elements, and easy access to reactant molecules on the NS surface make these materials especially useful for enzyme reactions requiring electron transfer, such as peroxidase. Furthermore, the peroxidase-like property of the $CeVO_4$ NS was exploited in the effective colorimetric detection of GSH with good sensitivity. The observed $K_M$ value for $CeVO_4$ NS (0.04 mM) is considerably lower than the previously reported $CeVO_4$ nanoparticles (3.52 mM)[56] and natural HRP. The low-temperature transition of the metal sulfides into the corresponding oxides provides a pathway for generating a wide variety of low-dimension structures. Overall, the method provides an entirely new synthetic strategy for the efficient and uniform synthesis of ultrathin $CeVO_4$ NS from non oxidic material, which can be used as a platform for nanozyme and sensor for biomolecule detection. The current synthesis process indicates new potential avenues of investigation for more fundamental research in this domain.

## EXPERIMENTAL METHODS

**Chemicals.** Cerium (III) nitrate hexahydrate (Ce $(NO_3)_3\cdot$ $6H_2O$), ammonium metavanadate ($NH_4VO_3$), ammonium hydroxide ($NH_4OH$), lithium hydroxide (LiOH), sodium chloride, sodium acetate, acetic acid, potassium chloride, uric acid, glutathione reduced (GSH), and lysine were purchased from SRL chemicals, India, and used without further purification. Native enzyme peroxidase from horseradish, hydrogen peroxide (30%), 3,3,5,5′-tetramethylbenzidine (TMB), sodium acetate, L-cysteine, ascorbic acid, urea, glucose, 4-nitrophenol, and phosphate-buffered saline (PBS) tablets were obtained from Sigma-Aldrich. Ultrapure Milli-Q water was used for all the experiments and preparation of buffers.

**Instrumentation.** UV−vis absorption spectra were recorded on a Varian UV−visible spectrophotometer at room temperature. Rigaku powder diffractometer (Cu K$\alpha$ radiation, $\lambda$ = 1.514 Å) was used to perform PXRD spectra. Raman spectroscopy measurement was performed using a Jobin Yvon Horiba LABRAM-HR system equipped with a 632.8 He−Ne laser beam. TEM and HRTEM images were recorded using Thermo Scientific, Themis 300 G3. JEOL JSM-7600F FEG-SEM with EDS attachment was used to collect SEM images. XPS (Axis Supra Model, SHIMADZU group) used to record XPS data.

**Synthesis of $CeVS_3$.** We synthesized $CeVS_3$ bulk sheets by solid-state synthesis. In a typical synthesis procedure, equal mmol of $NH_4VO_3$ and $Ce(NO_3)_3\cdot6H_2O$ were dissolved in 10 mL of Milli-Q water; then, 2 mL of $NH_4OH$ solution was added dropwise while stirring constantly for 15 min. After centrifuging the solution, the precipitate was collected in an alumina boat, which was then maintained in a tube furnace at 900 °C for 3 h. Ar and $H_2$ gases flowed through $CS_2$ at a rate of 40 and 10 sccm, respectively.

**Synthesis of $CeVO_4$ Nanosheets.** $CeVO_4$ nanosheets were chemically produced from $CeVS_3$ by the ion-intercalation exfoliation process in the presence of LiOH. In a typical experiment, 1 mmol of synthesized $CeVS_3$ was dissolved in 20 mL Milli-Q water, and 5 mmol of LiOH powder was added with constant stirring. The solution was stirred for 15 min before being placed in a Teflon-lined stainless steel autoclave with a 25 mL capacity and heated at 180 °C for 12 h. The product obtained from the reaction was sonicated in a bath sonicator for 30 min. It was then repeatedly rinsed with Milli-Q water before being washed with ethanol. The final product was dried in an oven at 80 °C for 8 h before being used for further characterization.

**Peroxidase-Mimicking Activity.** The enzyme mimicking activity of $CeVO_4$ NZ was investigated by performing the oxidation of TMB in the presence of $H_2O_2$. First, a $CeVO_4$ NZ stock solution of 2 mg/mL was prepared in Milli-Q water. In a typical experiment, TMB (0.1 mM) and $H_2O_2$ (2 mM) were added to sodium acetate buffer (100 mM, pH 4). Then, the aqueous suspension of $CeVO_4$ (25 $\mu$g/mL) was added, and the reaction mixture (total volume 1 mL) was kept at room temperature for 30 min.

To investigate the pH and temperature-dependent study, all the experiments were performed using $CeVO_4$ NZ (25 $\mu$g/mL), TMB (0.1 mM), and $H_2O_2$ (2 mM) in sodium acetate buffer (100 mM, pH 4). For the recyclability test, $CeVO_4$ NZ (1 mg/mL), TMB (0.1 mM), and $H_2O_2$ (2 mM) were taken in a 1 mL Eppendorf tube, and after 60 min, the centrifugation of

the reaction mixture was done at 6000 rpm for 15 min. Then, the UV–vis spectrum was recorded for the supernatant solution. Then the $CeVO_4$ NZ was washed with Milli-Q water, and again a catalytic reaction was performed. For glutathione detection, the catalytic reaction is performed by taking TMB (0.1 mM), $H_2O_2$ (2 mM), $CeVO_4$ (25 µg/mL), and GSH (varying concentration) in an acetate buffer (pH 4, 100 mM). The UV–vis spectra were recorded after 30 min incubation at 25 °C.

**Investigation of Enzyme Kinetic Parameters.** The catalytic efficiency of $CeVO_4$ was measured by taking UV–visible spectra at different time points. For the kinetic study, we performed the oxidation of varying concentrations of TMB (from 0.01 to 0.1 mM) in the presence of a fixed concentration of $H_2O_2$ (2 mM). We have also studied the $CeVO_4$ catalyzed oxidation of TMB (0.1 mM) in the presence of varying concentrations of $H_2O_2$ (from 0.02 to 0.1 mM) in an acetate buffer (100 mM, pH 4) at room temperature. The reaction kinetics were monitored by recording the absorbance at 652 nm for 30 min. To evaluate the kinetic parameters, the obtained data were fitted and plotted using the Michaelis–Menten and Lineweaver–Burk model (eq 1), where $K_M$ is the Michaelis–Menten constant, $V_{max}$ is the maximum velocity, $[S]$ is the substrate concentration, and $V$ is the velocity.

$$\frac{1}{V} = \left(\frac{K_M}{V_{max}}\right)\left(\frac{1}{[S]}\right) + \left(\frac{1}{V_{max}}\right) \tag{1}$$

## ASSOCIATED CONTENT

**ⓢ Supporting Information**

The Supporting Information is available free of charge at https://pubs.acs.org/doi/10.1021/acsomega.2c07732.

EDS spectrum of $CeVS_3$; full range survey spectrum of $CeVO_4$ nanosheets; zeta potential data; UV–vis spectra of $CeVO_4$ catalyzed reactions; SEM image and XRD data of $CeVO_4$ nanosheets (before and after catalysis); concentration-dependent peroxidase mimicking activity data; and experimental results in tabular form (PDF)

## AUTHOR INFORMATION

**Corresponding Author**

**Siddarth Jain** − *Department of Chemistry, Indian Institute of Technology Bombay, Mumbai 400076, India;* ⓞ orcid.org/0000-0003-3829-5249; Email: jainsiddarth477@gmail.com

**Authors**

**Kuldeep Kumar** − *Department of Chemistry, Indian Institute of Technology Bombay, Mumbai 400076, India;* ⓞ orcid.org/0000-0002-3481-0322

**Tanmoy Maity** − *Indian Institute of Science Education and Research Kolkata, Nadia, West Bengal 741246, India*

**Leela S. Panchakarla** − *Department of Chemistry, Indian Institute of Technology Bombay, Mumbai 400076, India;* ⓞ orcid.org/0000-0001-5829-3377

Complete contact information is available at:
https://pubs.acs.org/10.1021/acsomega.2c07732

**Author Contributions**

K.K., L.S.P., and S.J. conceptualized the project; all the materials synthesis and characterizations were done by K.K.; T.M. and S.J. performed the peroxidase mimic activity experiments; K.K., T.M., and S.J. analyzed the data; K.K., T.M., and S.J. wrote the manuscript; K.K. and S.J. revised and edited the manuscript; L.S.P and S.J. supervised the project.

**Notes**

The authors declare no competing financial interest.

## REFERENCES

(1) Geim, A. K.; Novoselov, K. S. The Rise of Graphene. *Nat. Mater.* **2007**, *6*, 183−191.

(2) Zhu, Y.; Murali, S.; Cai, W.; Li, X.; Suk, J. W.; Potts, J. R.; Ruoff, R. S. Graphene and Graphene Oxide: Synthesis, Properties, and Applications. *Adv. Mater.* **2010**, *22*, 3906−3924.

(3) Beladi-Mousavi, S. M.; Khezri, B.; Krejčová, L.; Heger, Z.; Sofer, Z.; Fisher, A. C.; Pumera, M. Recoverable Bismuth-Based Micro-robots: Capture, Transport, and On-Demand Release of Heavy Metals and an Anticancer Drug in Confined Spaces. *ACS Appl. Mater. Interfaces* **2019**, *11*, 13359−13369.

(4) Baig, N. Two-Dimensional Nanomaterials: A Critical Review of Recent Progress, Properties, Applications, and Future Directions. *Compos. Appl. Sci. Manuf.* **2023**, *165*, 107362.

(5) Chhowalla, M.; Shin, H. S.; Eda, G.; Li, L.-J.; Loh, K. P.; Zhang, H. The Chemistry of Two-Dimensional Layered Transition Metal Dichalcogenide Nanosheets. *Nat. Chem.* **2013**, *5*, 263−275.

(6) Wang, Q. H.; Kalantar-Zadeh, K.; Kis, A.; Coleman, J. N.; Strano, M. S. Electronics and Optoelectronics of Two-Dimensional Transition Metal Dichalcogenides. *Nat. Nanotechnol.* **2012**, *7*, 699−712.

(7) Ma, R.; Sasaki, T. Two-Dimensional Oxide and Hydroxide Nanosheets: Controllable High-Quality Exfoliation, Molecular Assembly, and Exploration of Functionality. *Acc. Chem. Res.* **2015**, *48*, 136−143.

(8) Coleman, J. N.; Lotya, M.; O'Neill, A.; Bergin, S. D.; King, P. J.; Khan, U.; Young, K.; Gaucher, A.; De, S.; Smith, R. J.; Shvets, I. V.; Arora, S. K.; Stanton, G.; Kim, H.-Y.; Lee, K.; Kim, G. T.; Duesberg, G. S.; Hallam, T.; Boland, J. J.; Wang, J. J.; Donegan, J. F.; Grunlan, J. C.; Moriarty, G.; Shmeliov, A.; Nicholls, R. J.; Perkins, J. M.; Grieveson, E. M.; Theuwissen, K.; McComb, D. W.; Nellist, P. D.; Nicolosi, V. Two-Dimensional Nanosheets Produced by Liquid Exfoliation of Layered Materials. *Science* **2011**, *331*, 568−571.

(9) Wang, Q.; O'Hare, D. Recent Advances in the Synthesis and Application of Layered Double Hydroxide (LDH) Nanosheets. *Chem. Rev.* **2012**, *112*, 4124−4155.

(10) Ma, R.; Liang, J.; Liu, X.; Sasaki, T. General Insights into Structural Evolution of Layered Double Hydroxide: Underlying Aspects in Topochemical Transformation from Brucite to Layered Double Hydroxide. *J. Am. Chem. Soc.* **2012**, *134*, 19915−19921.

(11) Gangadharan, D. T.; Ma, D. Searching for Stability at Lower Dimensions: Current Trends and Future Prospects of Layered Perovskite Solar Cells. *Energy Environ. Sci.* **2019**, *12*, 2860−2889.

(12) Li, X.; Hoffman, J. M.; Kanatzidis, M. G. The 2D Halide Perovskite Rulebook: How the Spacer Influences Everything from the Structure to Optoelectronic Device Efficiency. *Chem. Rev.* **2021**, *121*, 2230−2291.

(13) Leung, T. L.; Ahmad, I.; Syed, A. A.; Ng, A. M. C.; Popović, J.; Djurišić, A. B. Stability of 2D and Quasi-2D Perovskite Materials and Devices. *Commun. Mater.* **2022**, *3*, 1−10.

(14) Liu, P.; Yu, S.; Xiao, S. Research progress on two-dimensional (2D) halide organic-inorganic hybrid perovskites. *Sustain. Energy Fuels* **2021**, *5*, 3950−3978.

(15) Novoselov, K. S.; Jiang, D.; Schedin, F.; Booth, T. J.; Khotkevich, V. V.; Morozov, S. V.; Geim, A. K. Two-Dimensional Atomic Crystals. *Proc. Natl. Acad. Sci. USA* **2005**, *102*, 10451−10453.

(16) Chia, H. L.; Mayorga-Martinez, C. C.; Pumera, M. Doping and Decorating 2D Materials for Biosensing: Benefits and Drawbacks. *Adv. Funct. Mater.* **2021**, *31*, 2102555.

(17) Yuan, C.; Wu, H. B.; Xie, Y.; Lou, X. W. Mixed Transition-Metal Oxides: Design, Synthesis, and Energy-Related Applications. *Angew. Chem., Int. Ed.* **2014**, *53*, 1488−1504.

(18) Yang, Z.; Zhao, L.; Zhang, S.; Zhao, X. Ferroelectric-Enhanced $BiVO_4$-$BiFeO_3$ Photoelectrocatalysis for Efficient, Stable and Large-Current-Density Oxygen Evolution. *Appl. Mater. Today* **2022**, *26*, 101374.

(19) Villa, K.; Novotný, F.; Zelenka, J.; Browne, M. P.; Ruml, T.; Pumera, M. Visible-Light-Driven Single-Component $BiVO_4$ Micromotors with the Autonomous Ability for Capturing Microorganisms. *ACS Nano* **2019**, *13*, 8135−8145.

(20) Liang, Y.; Wang, H.; Zhou, J.; Li, Y.; Wang, J.; Regier, T.; Dai, H. Covalent Hybrid of Spinel Manganese-Cobalt Oxide and Graphene as Advanced Oxygen Reduction Electrocatalysts. *J. Am. Chem. Soc.* **2012**, *134*, 3517−3523.

(21) Cheng, F.; Shen, J.; Peng, B.; Pan, Y.; Tao, Z.; Chen, J. Rapid Room-Temperature Synthesis of Nanocrystalline Spinels as Oxygen Reduction and Evolution Electrocatalysts. *Nat. Chem.* **2011**, *3*, 79−84.

(22) Xiong, P.; Liu, B.; Teran, V.; Zhao, Y.; Peng, L.; Wang, X.; Yu, G. Chemically Integrated Two-Dimensional Hybrid Zinc Manganate/Graphene Nanosheets with Enhanced Lithium Storage Capability. *ACS Nano* **2014**, *8*, 8610−8616.

(23) Xiong, P.; Peng, L.; Chen, D.; Zhao, Y.; Wang, X.; Yu, G. Two-Dimensional Nanosheets Based Li-Ion Full Batteries with High Rate Capability and Flexibility. *Nano Energy* **2015**, *12*, 816−823.

(24) Song, Q.; Zhang, Z. J. Controlled Synthesis and Magnetic Properties of Bimagnetic Spinel Ferrite $CoFe_2O_4$ and $MnFe_2O_4$ Nanocrystals with Core−Shell Architecture. *J. Am. Chem. Soc.* **2012**, *134*, 10182−10190.

(25) Zeng, H.; Rice, P. M.; Wang, S. X.; Sun, S. Shape-Controlled Synthesis and Shape-Induced Texture of $MnFe_2O_4$ Nanoparticles. *J. Am. Chem. Soc.* **2004**, *126*, 11458−11459.

(26) Liu, B.; Zhang, J.; Wang, X.; Chen, G.; Chen, D.; Zhou, C.; Shen, G. Hierarchical Three-Dimensional $ZnCo_2O_4$ Nanowire Arrays/Carbon Cloth Anodes for a Novel Class of High-Performance Flexible Lithium-Ion Batteries. *Nano Lett.* **2012**, *12*, 3005−3011.

(27) Huang, L.; Chen, D.; Ding, Y.; Feng, S.; Wang, Z. L.; Liu, M. Nickel−Cobalt Hydroxide Nanosheets Coated on $NiCo_2O_4$ Nanowires Grown on Carbon Fiber Paper for High-Performance Pseudocapacitors. *Nano Lett.* **2013**, *13*, 3135−3139.

(28) Hu, L.; Zhong, H.; Zheng, X.; Huang, Y.; Zhang, P.; Chen, Q. $CoMn_2O_4$ Spinel Hierarchical Microspheres Assembled with Porous Nanosheets as Stable Anodes for Lithium-Ion Batteries. *Sci. Rep.* **2012**, *2*, 986.

(29) Zhu, Y.; Cao, C.; Zhang, J.; Xu, X. Two-Dimensional Ultrathin $ZnCo_2O_4$ Nanosheets: General Formation and Lithium Storage Application. *J. Mater. Chem. A* **2015**, *3*, 9556−9564.

(30) Sun, Z.; Liao, T.; Dou, Y.; Hwang, S. M.; Park, M.-S.; Jiang, L.; Kim, J. H.; Dou, S. X. Generalized Self-Assembly of Scalable Two-Dimensional Transition Metal Oxide Nanosheets. *Nat. Commun.* **2014**, *5*, 3813.

(31) Tao, P.; Yao, S.; Liu, F.; Wang, B.; Huang, F.; Wang, M. Recent Advances in Exfoliation Techniques of Layered and Non-Layered Materials for Energy Conversion and Storage. *J. Mater. Chem. A* **2019**, *7*, 23512−23536.

(32) Mosleh, M.; Mahinpour, A. Sonochemical Synthesis and Characterization of Cerium Vanadate Nanoparticles and Investigation

(33) Ashrafi, S.; Mousavi-Kamazani, M.; Zinatloo-Ajabshir, S.; Asghari, A. Novel Sonochemical Synthesis of $Zn_2V_2O_7$ Nanostructures for Electrochemical Hydrogen Storage. *Int. J. Hydrogen Energy* **2020**, *45*, 21611−21624.

(34) Song, J.; Wu, F.; Lu, Y.; Zhang, X.; Li, Z. $CeVO_4$/$CeO_2$ Heterostructure-Supported Co Nanoparticles for Photocatalytic $H_2$ Production from Ammonia Borane under Visible Light. *ACS Appl. Nano Mater.* **2021**, *4*, 4800−4809.

(35) Kokulnathan, T.; Sakthi Priya, T.; Wang, T.-J. Surface Engineering Three-Dimensional Flowerlike Cerium Vanadate Nanostructures Used as Electrocatalysts: Real Time Monitoring of Clioquinol in Biological Samples. *ACS Sustain. Chem. Eng.* **2019**, *7*, 16121−16130.

(36) Wang, H.; Meng, Y.; Yan, H. Rapid Synthesis of Nanocrystalline $CeVO_4$ by Microwave Irradiation. *Inorg. Chem. Commun.* **2004**, *7*, 553−555.

(37) Chia, H. L.; Mayorga-Martinez, C. C.; Gusmão, R.; Novotny, F.; Webster, R. D.; Pumera, M. A Highly Sensitive Enzyme-Less Glucose Sensor Based on Pnictogens and Silver Shell−Gold Core Nanorod Composites. *Chem. Commun.* **2020**, *56*, 7909−7912.

(38) Phuruangrat, A.; Kuntalue, B.; Thongtem, S.; Thongtem, T. Effect of PEG on Phase, Morphology and Photocatalytic Activity of $CeVO_4$ Nanostructures. *Mater. Lett.* **2016**, *174*, 138−141.

(39) Fan, C.; Liu, Q.; Ma, T.; Shen, J.; Yang, Y.; Tang, H.; Wang, Y.; Yang, J. Fabrication of 3D $CeVO_4$/Graphene Aerogels with Efficient Visible-Light Photocatalytic Activity. *Ceram. Int.* **2016**, *42*, 10487−10492.

(40) Zhu, L.; Li, Q.; Li, J.; Liu, X.; Meng, J.; Cao, X. Selective Synthesis of Mesoporous and Nanorod $CeVO_4$ without Template. *J. Nanoparticle Res.* **2007**, *9*, 261−268.

(41) Liu, F.; Shao, X.; Yin, Y.; Zhao, L.; Shao, Z.; Liu, X.; Meng, X. Shape Controlled Synthesis and Tribological Properties of $CeVO_4$ Nanoparticles Aslubricating Additive. *J. Rare Earths* **2011**, *29*, 688−691.

(42) Chen, L. Hydrothermal Synthesis and Ethanol Sensing Properties of $CeVO_4$ and $CeVO_4$−$CeO_2$ Powders. *Mater. Lett.* **2006**, *60*, 1859−1862.

(43) Picardi, G.; Varsano, F.; Decker, F.; Opara-Krasovec, U.; Surca, A.; Orel, B. Electrochemical Characterization of Optically Passive $CeVO_4$ Counterelectrodes. *Electrochim. Acta* **1999**, *44*, 3157−3164.

(44) Zonarsaghar, A.; Mousavi-Kamazani, M.; Zinatloo-Ajabshir, S. Hydrothermal Synthesis of $CeVO_4$ Nanostructures with Different Morphologies for Electrochemical Hydrogen Storage. *Ceram. Int.* **2021**, *47*, 35248−35259.

(45) Bai, J.; Han, S.-H.; Peng, R.-L.; Zeng, J.-H.; Jiang, J.-X.; Chen, Y. Ultrathin Rhodium Oxide Nanosheet Nanoassemblies: Synthesis, Morphological Stability, and Electrocatalytic Application. *ACS Appl. Mater. Interfaces* **2017**, *9*, 17195−17200.

(46) Shu, X.; Zheng, H.; Xu, G.; Zhao, J.; Cui, L.; Cui, J.; Qin, Y.; Wang, Y.; Zhang, Y.; Wu, Y. The Anodization Synthesis of Copper Oxide Nanosheet Arrays and Their Photoelectrochemical Properties. *Appl. Surf. Sci.* **2017**, *412*, 505−516.

(47) Wolfenden, R.; Snider, M. J. The Depth of Chemical Time and the Power of Enzymes as Catalysts. *Acc. Chem. Res.* **2001**, *34*, 938−945.

(48) Huang, Y.; Ren, J.; Qu, X. Nanozymes: Classification, Catalytic Mechanisms, Activity Regulation, and Applications. *Chem. Rev.* **2019**, *119*, 4357−4412.

(49) Wu, J.; Wang, X.; Wang, Q.; Lou, Z.; Li, S.; Zhu, Y.; Qin, L.; Wei, H. Nanomaterials with Enzyme-like Characteristics (Nanozymes): Next-Generation Artificial Enzymes (II). *Chem. Soc. Rev.* **2019**, *48*, 1004−1076.

(50) Jiang, D.; Ni, D.; Rosenkrans, Z. T.; Huang, P.; Yan, X.; Cai, W. Nanozyme: New Horizons for Responsive Biomedical Applications. *Chem. Soc. Rev.* **2019**, *48*, 3683−3704.

(51) Wang, H.; Wan, K.; Shi, X. Recent Advances in Nanozyme Research. *Adv. Mater.* **2019**, *31*, 1805368.

(52) Maity, T.; Jain, S.; Solra, M.; Barman, S.; Rana, S. Robust and Reusable Laccase Mimetic Copper Oxide Nanozyme for Phenolic Oxidation and Biosensing. *ACS Sustain. Chem. Eng.* **2022**, *10*, 1398–1407.

(53) Rohaizad, N.; Mayorga-Martinez, C. C.; Fojtů, M.; Latiff, N. M.; Pumera, M. Two-Dimensional Materials in Biomedical, Biosensing and Sensing Applications. *Chem. Soc. Rev.* **2021**, *50*, 619–657.

(54) Yang, Y.; Mao, Z.; Huang, W.; Liu, L.; Li, J.; Li, J.; Wu, Q. Redox Enzyme-Mimicking Activities of $CeO_2$ Nanostructures: Intrinsic Influence of Exposed Facets. *Sci. Rep.* **2016**, *6*, 35344.

(55) Ju, P.; Yu, Y.; Wang, M.; Zhao, Y.; Zhang, D.; Sun, C.; Han, X. Synthesis of EDTA-Assisted $CeVO_4$ Nanorods as Robust Peroxidase Mimics towards Colorimetric Detection of $H_2O_2$. *J. Mater. Chem. B* **2016**, *4*, 6316–6325.

(56) Jain, S.; Sharma, B.; Thakur, N.; Mishra, S.; Sarma, T. K. Copper Pyrovanadate Nanoribbons as Efficient Multienzyme Mimicking Nanozyme for Biosensing Applications. *ACS Appl. Nano Mater.* **2020**, *3*, 7917–7929.

(57) Qian, X.; Wang, Y.; Ju, Z.; Xie, M.; Zhang, B.; Yu, G. Chemical Exfoliation of Metal Oxide Nanosheets for High-Performance Ion Conducting Membranes. *ACS Mater. Lett.* **2022**, *4*, 2321–2327.

(58) Singh, N.; Mugesh, G. $CeVO_4$ Nanozymes Catalyze the Reduction of Dioxygen to Water without Releasing Partially Reduced Oxygen Species. *Angew. Chem., Int. Ed.* **2019**, *58*, 7797–7801.

(59) Othman, I.; Hisham Zain, J.; Abu Haija, M.; Banat, F. Catalytic Activation of Peroxymonosulfate Using $CeVO_4$ for Phenol Degradation: An Insight into the Reaction Pathway. *Appl. Catal., B* **2020**, *266*, 118601.

(60) Tripathi, V.; Jain, S.; Kabra, D.; Panchakarla, L. S.; Dutta, A. Cobalt-Doped Copper Vanadate: A Dual Active Electrocatalyst Propelling Efficient $H_2$ Evolution and Glycerol Oxidation in Alkaline Water. *Nanoscale Adv.* **2022**, *5*, 237–246.

(61) Bocan, J.; Sidorová, M.; Sofranko, M. Thermodynamic Study of Metal Sulphides Conversion to Oxides in Hydrometallurgy. *Metalurgija* **2017**, *56*, 157–160.

(62) Kim, T. I.; Kim, J.; Park, I.-J.; Cho, K.-O.; Choi, S.-Y. Chemically Exfoliated 1T-Phase Transition Metal Dichalcogenide Nanosheets for Transparent Antibacterial Applications. *2D Mater.* **2019**, *6*, 025025.

(63) Shuai, J.; Yoo, H. D.; Liang, Y.; Li, Y.; Yao, Y.; Grabow, L. C. Density Functional Theory Study of Li, Na, and Mg Intercalation and Diffusion in $MoS_2$ with Controlled Interlayer Spacing. *Mater. Res. Express* **2016**, *3*, 064001.

(64) Dai, H.; Zhao, Y.; Zhang, Z.; Yang, J.; Liu, S.; Zhou, J.; Sun, G. Ostwald Ripening and Sulfur Escaping Enabled Chrysanthemum-like Architectures Composed of $NiS_2$/NiS@C Heterostructured Petals with Enhanced Charge Storage Capacity and Rate Capability. *J. Electroanal. Chem.* **2022**, *921*, 116671.

(65) Zhang, Q.; Mei, L.; Cao, X.; Tang, Y.; Zeng, Z. Intercalation and Exfoliation Chemistries of Transition Metal Dichalcogenides. *J. Mater. Chem. A* **2020**, *8*, 15417–15444.

(66) Cai, S.; Yang, R. Two-Dimensional Nanomaterials With Enzyme-Like Properties for Biomedical Applications. *Front. Chem.* **2020**, *8*, 565940.

(67) Sun, Y.; Xu, H.; Zhao, X.; Hui, Z.; Yu, C.; Wang, L.; Xue, J.; Zhao, Y.; Zhou, R.; Dai, H.; Miao, C.; Chen, Q.; Zhou, J.; Sun, G.; Huang, W. Identifying the Active Site of Ultrathin NiCo LDH as an Efficient Peroxidase Mimic with Superior Substrate Affinity for Sensitive Detection of Hydrogen Peroxide. *J. Mater. Chem. B* **2019**, *7*, 6232–6237.

(68) Sun, Y.; Xu, H.; Wang, L.; Yu, C.; Zhou, J.; Chen, Q.; Sun, G.; Huang, W. Ultrathin NiMn Layered Double Hydroxide Nanosheets with a Superior Peroxidase Mimicking Performance to Natural HRP for Disposable Paper-Based Bioassays. *J. Mater. Chem. B* **2021**, *9*, 983–991.

(69) Yang, Y.; Dai, H.; Sun, Y.; Wang, L.; Qin, G.; Zhou, J.; Chen, Q.; Sun, G. 2D material-based peroxidase-mimicking nanozymes: catalytic mechanisms and bioapplications. *Anal. Bioanal. Chem.* **2022**, *414*, 2971–2989.

(70) Yang, H.; Zha, J.; Zhang, P.; Qin, Y.; Chen, T.; Ye, F. Fabrication of $CeVO_4$ as Nanozyme for Facile Colorimetric Discrimination of Hydroquinone from Resorcinol and Catechol. *Sens. Actuators, B* **2017**, *247*, 469–478.

(71) Bernard, P.; Stelmachowski, P.; Broś, P.; Makowski, W.; Kotarba, A. Demonstration of the Influence of Specific Surface Area on Reaction Rate in Heterogeneous Catalysis. *J. Chem. Educ.* **2021**, *98*, 935–940.

(72) Liu, B.; Wang, Y.; Chen, Y.; Guo, L.; Wei, G. Biomimetic Two-Dimensional Nanozymes: Synthesis, Hybridization, Functional Tailoring, and Biosensor Applications. *J. Mater. Chem. B* **2020**, *8*, 10065–10086.

(73) Ren, X.; Chen, D.; Wang, Y.; Li, H.; Zhang, Y.; Chen, H.; Li, X.; Huo, M. Nanozymes-Recent Development and Biomedical Applications. *J. Nanobiotechnol.* **2022**, *20*, 92.

(74) Jain, S.; Panigrahi, A.; Sarma, T. K. Counter Anion-Directed Growth of Iron Oxide Nanorods in a Polyol Medium with Efficient Peroxidase-Mimicking Activity for Degradation of Dyes in Contaminated Water. *ACS Omega* **2019**, *4*, 13153–13164.

(75) Ma, Q.; Wang, M.; Cai, H.; Li, F.; Fu, S.; Liu, Y.; Zhao, Y. A Sensitive and Rapid Detection of Glutathione Based on a Fluorescence-Enhanced "Turn-on" Strategy. *J. Mater. Chem. B* **2021**, *9*, 3563–3572.